Desalination and Water Treatment
www.deswater.com

doi:10.5004/dwt.2017.20718

72 (2017) 360–367
April

Rare earth elements/WO_3 nanowires: Visible lights nanophotocatalysts

R.M. Mohamed[a,b,*], E.S. Aazam[a], Z.A. Aldabbagh[a,c]

[a]*Chemistry department, Faculty of Science, King Abdul Aziz university, Jeddah, KSA, PO Box 80203 21589 Jeddah, Saudi Arabia, email: redama123@yahoo.com (R.M. Mohamed), elhamaazam@gmail.com (E.S. Aazam)*
[b]*Nanostructured Material Division Advanced Materials Department, Central Metallurgical R&D Institute, Helwan, 11421, Cairo, Egypt*
[c]*Center of Excellence in Environmental Studies, King Abdulaziz University, P.O. Box 80216, Jeddah 21589, Saudi Arabia, email: zain404@hotmail.com (Z.A. Aldabbagh)*

Received 23 December 2016; Accepted 17 March 2017

ABSTRACT

Tungsten trioxide nanowires were prepared successfully by a sol- gel technique. Rare earth doped tungsten trioxide nanowires were successfully prepared by a photoassisted deposition route. Tungsten trioxide and rare earth doped tungsten trioxide nanowires were characterized by many characterization methods. The XRD results reveal that all tungsten trioxide and rare earth doped tungsten trioxide nanowires samples are composed of WO_3 form. Also, we noticed that the intensity of tungsten trioxide sample is higher than that of rare earth doped tungsten trioxide nanowires samples, which means rare earth elements can retard grain growth of WO_3 particles. Nd-WO_3 photocatalyst has the lowest crystallite size and band gap and has highest photocatalytic activity and specific surface area in regard to other rare earth doped WO_3 samples. This can be attributed to its individual properties of crystallite size , band gap and surface of texture. Details of the preparation process and outcomes of characterizations of the prepared rare earth doped tungsten trioxide nanowires are discussed.

Keywords: Tungsten trioxide; Rare earth; Thiophene

1. Introduction

Removal of sulphur from fluidized catalytic cracker (FCC) naphtha up to the favorable limits is a critical issue in the refining industry. The FCC naphtha is a major component of gasoline pool. The main sulfur containing compounds present in FCC naphtha are the thiophenes. Thiophenes are aromatic compounds and so they are inert relative to other sulphur-containing compounds. Hydrodesulfurization process is one of the important methods that have been used in removal of thiophenes [1–8].

The draw backs of this method are its high cost besides, affecting the octane number of gasoline. Many alternative efficient and economical methods have been investigated, for removal of thiophene compounds, to overcome these draws backs such as pervaporation method [9–13]. Temperature and pressure requirements in pervaporation are relatively low in comparison to hydrodesulfurization and it was concluded that the pervaporation method remove thiophene successfully from FCC gasoline up to any favorable limit. Several alternative processes have also been reported for thiophene removal, such as reactive adsorption using solid adsorbents and H_2 [14], selective adsorption without H_2 at ambient temperature [15–21], hydrodesulfurization with distillation [22,23], absorption with ionic liquids [24–26]. Although the broad scale applications of these processes but they are very costly.

Recently, different polymeric materials such as polyhedral oligomeric silsesquioxane (POSS), poly vinylidene fluoride (PVDF), polyimide (PI), poly ethylene glycol (PEG), etc…. have been used as membrane material for thiophene removal from gasoline [27–39]. In modern trends, extraction desulfurization has been devoted to be the most effective and suitable method as a result of its mild operational conditions of temperature and pressure without any hydrogen consumption [40].

*Corresponding author.

In recent years, there has been an extensive interest in heterogeneous photocatalysis using semiconductors for the removal of pollutants. The main advantage of photocatalysis is that it provides a more environmentally sustainable solution for pollutant removal without any need for further treatment. The degradation of thiophene under visible-light irradiation using nanocomposites made of polyaniline/mesoporous Cu_2O was studied [41]. The photocatalytic efficiency of a semiconductor/conductive polymer composite under visible light is large.TiO_2 was doped with Ag and the resulted photocatalyst was supported on MWCNTs, and then Ag–TiO_2/ MWCNT photocatalysts were used to degrade thiophene by photocatalysis under visible light irradiation in an aqueous solution and it was found that the optimum mass ratio of MWCNT:TiO_2: Ag was 0.02:1.0:0.05, which resulted in the photo catalyst's experimental performance in oxidizing about 100% of the thiophene in a 600 mg/L solution within 30 min [42]. Other researchers studied the photo oxidation of thiophene using different materials as, RuO_2/SO_2-TiO_2 [43], NiO/$AgInS_2$ nanoparticles [44], Pd/ZrO_2–chitosan nanocomposite [45], Ag–$BiVO_4$ [46], TiO_2/Cr-MCM-41 [47], TiO_2 [48], TiO_2/Ni-ZSM-5 [49]. Pt/PbS Nanoparticles [50], MoO_3/ɤ-Al_2O_3 [51], titania/MWCNT composite [52].

Tungsten trioxide is narrow band gap [53]. Tungsten trioxide photocatalysts can be prepared by many methods [54–60]. The drawbacks for using tungsten trioxide as photocatalyst is high electron-hole recombination rate and low specific surface area, many methods were used to improve photocatalytic activity of tungsten trioxide such as by nitrogen doping [61,62]. In this paper, tungsten trioxide was prepared by a sol-gel method in presence of surfactant to improve its specific surface area and also, we studied effect of different rare earth elements on rate of electron-hole recombination and studied its photocatalytic activity for removal of thiophene under visible light.

2. Experimental

2.1. Synthesis of the photocatalysts

The precursors were used in the sol-gel preparations of tungsten trioxide are tungsten isopropoxide, glycine, propanol, titanium isoperoxide, erbium nitrate, praseodymium nitrate, europium nitrate, and neodymium nitrate. The sol-gel method was employed to prepare WO_3 nanowires. In this procedure, 6.0 g of glycine was dissolved in a mixture of 30 mL of distilled water, 20 mL propanol and 0.05 g of 1 M HNO_3. 20.0 g of tungsten isopropoxide was added to the mixture. After stirring for 60 min at room temperature, the resulting mixture was left to stand until the formation of gel. The gel was then calcined in air for 5 h at 550°C.

Rare earth doped tungsten trioxide nanowires were successfully prepared by a photoassisted deposition route as in the following steps: dispersion of WO_3 nanowire in water, then dissolving of required amount of rare earth elements, in the suspension. To remove any dissolved oxygen in the suspension, the suspension was bubbled by nitrogen gas for 1 h and rate of 100 ml per minute. The suspension was irradiated for 24 h using Hg–Xe lamp. The photo generated electrons can reduced Er, Eu, Pr and Nd ions to Er, Eu, Pr and Nd metals and there were deposited on surface of WO_3 nanowire. The Rare earth doped tungsten trioxide nanowires samples were washed and dried in air for 2 h at 100°C. The weight percent of WO_3 to rare earth elements were kept as 98 to 2 wt %.

2.2. Characterisation techniques

The nanostructure of the prepared materials were examined by the mean of JEOL-JEM-1230 Transmission electron microscope (TEM). A Nova 2000 series Chromatech apparatus was employed to determine the prepared materials specific surface area. Bruker axis D8 with Cu Kα radiation (λ = 1.540 Å) was applied to determine the prepared materials phase and their crystallite size. A Thermo Scientific K-ALPHA spectrometer was applied to determine state of the prepared materials. A spectrophotometer of type (V-570, Jasco, Japan) was adopted to determine the band gap of the synthesized materials. A fluorescence spectrophotometer (Shimadzu RF-5301) was applied to determine the prepared materials emission spectra.

2.3. Photocatalytic experiment

Rare earth elements/WO_3 nanowires were used to measure degradation of thiophene using Visible light. Annular batch reactor with a horizontal cylinder was used for the photocatalytic reaction. A blue fluorescent lamp, which has 150 W as power and maximum energy corresponding to 450 nm and covered by UV cut filter, was used to irradiate rare earth elements/ WO_3 nanowires photocatalysts. Rare earth elements/ WO_3 nanowires photocatalysts were dispersed in acetonitrile solution containing thiophene ([sulfur content] initial = 600 ppm). The photocatalytic reactions were carried out at 12°C by a flow of cooling water. Sample from reaction mixture was taken at interval times to measure the photocatalytic activity of rare earth elements/WO_3 nanowires. The samples were analyzed by GC, Agilent 7890 and GC-MS to determine the thiophene remaining concentration in the reaction mixture. GC conditions applied for photocatalytic oxidation of thiophene are summarized in Table 1.

Table 1
Chromatographic conditions applied for photocatalytic oxidation of thiophene

	Oxidation of thiophene
Oven	35°C for 2 min, 35–80°C at 10°C/min, 80°C for 6 min, 80–220°C at 15°C/min, 220°C for 10 min
Carrier detector	Helium, constant pressure mode, 8.6 psi
Sample loop	Agilent 355 SCD Burner temperature: 800°C Vacuum of burner: 350 Torr Vacuum of reaction cell: 5 Torr Air flow: 60 ml/min H_2 flow: 40 ml/min 1 mL
Inlet	Inert flow path split/splitless inlet, 240°C, split ratio 10:1
Column	Agilent J&W DB-Sulfur SCD, 70 m × 0.53 mm, 4.3 µm

The removal efficiency of thiophene was measured by adopting the following equation:

$$\% \text{ Removal efficiency} = (C_o - C)/C_o \times 1001) \quad (1)$$

where C_o is the initial concentration of thiophene and C is the remaining concentration of thiophene.

2.4. Photocurrent intensity tests

Boiling TIO (Indium-tin-oxide) slices in sodium hydroxide solution (2M) and deionized water, alcohol and acetone were used for sonication of the ITO for 15 min. After that, TIO was dried at room temperature. The pretreated ITO was dropped in WO_3 nanowires or rare earth elements/WO_3 nanowires solutions. Electrochemical workstation, Zahner Zennium, Germany was used to record photocurrent intensity in Na_2SO_4 solution (0.1 M) and 0.2 V applied potential. The irradiation source is a 500 W, Xe lamp and it was connect to a monochromator to produce the monochromatic light at 420 nm.

3. Results and discussion

3.1. Photocatalysts characterizations

Fig. 1. shows XRD patterns of tungsten trioxide and rare earth doped tungsten trioxide nanowires. The XRD results reveal that all tungsten trioxide and rare earth doped tungsten trioxide nanowires samples are composed of WO_3 form. Also, we noticed that the intensity of tungsten trioxide sample is higher than that of rare earth doped tungsten trioxide nanowires samples, which means rare earth elements can retard grain growth of WO_3 particles. Also, we noticed that there is no diffraction peaks for rare earth or rare earth oxides, which may be due to low content of rare earth element or may be due to high dispersion of rare earth on surface of tungsten trioxide nanowires. Scherrer

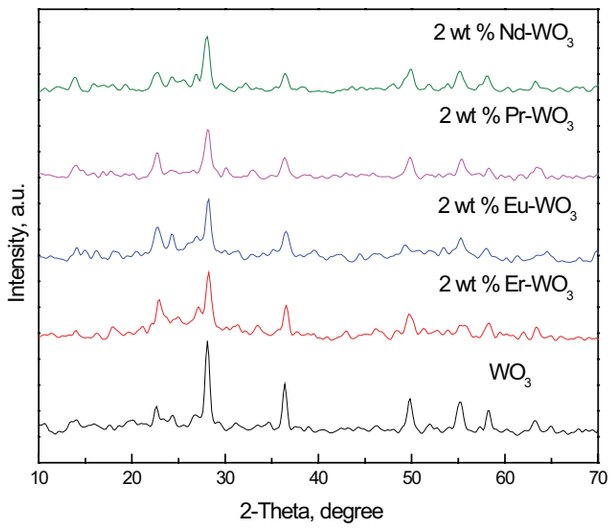

Fig. 1. XRD patterns of tungsten trioxide and rare earth doped tungsten trioxide nanowires.

equation was used to calculate crystallite size of tungsten trioxide and rare earth doped tungsten trioxide samples. The crystallite size for WO_3, Er-WO_3, Eu-WO_3, Pr-WO_3 and Nd-WO_3 samples is 20, 18, 16, 14 and 12 nm, respectively. Therefore, doping of rare earth elements can retard grain growth of WO_3 particles.

Fig. 2. shows that XPS spectra of W, O, Er, Eu, Pr and Nd species of rare earth doped tungsten trioxide nanowires samples. The presence of two binding energy at 36.6 and 34.6 eV for $W4f_{5/2}$ and $W4f_{7/2}$, respectively, prove the existence of W^{6+} ions, as shown in Fig. 2A. The presence of one binding energy at 531.4 eV for O1s , prove the existence of O^{2-} ions, as shown in Fig. 2B. The presence of W^{6+} and O^{2-} ions , prove the existence of WO_3, which agree with XRD results. The presence of two binding energy at 1126 and 1165 eV for $Eu3d_{5/2}$ and $Eu3d_{3/2}$, respectively, prove the existence of metallic europium , as shown in Fig. 2C. The presence of one binding energy at 167.5 eV for prove the existence of metallic erbium, as shown in Fig. 2D. The presence of two binding energy at 932 and 954 eV for Pr $3d_{5/2}$ and Pr $d_{3/2}$, respectively, prove the existence of metallic praseodymium , as shown in Fig. 2E. The presence of two binding energy at 981.4 and 1006 eV for Nd $3d_{5/2}$ and Nd $d_{3/2}$, respectively, prove the existence of metallic neodymium, as shown in Fig. 2F.

Fig. 3 shows TEM image of tungsten trioxide and 2 wt % Nd-WO_3 nanowires. The results reveal that the shape of WO_3 and Nd-WO_3 samples is nanowires, which means deposition of rare earth has no significant effect on shape of WO_3. Also, we noticed that rare earth (neodymium) was deposited as dots on surface of WO_3 nanowires.

The BET surface area of tungsten trioxide and rare earth doped tungsten trioxide nanowires are tabulated in Table 2. The BET surface area values are 90, 87, 86, 85 and 89 m^2/g, for WO_3, Er-WO_3, Eu-WO_3, Pr-WO_3 and Nd-WO_3 samples. The BET values of tungsten trioxide and rare earth doped tungsten trioxide nanowires are higher than other samples mentioned in literature, due to using of glycerin as structure directing agent. Also, we noticed that doping of rare earth element may be block some pores of tungsten trioxide and so BET surface area of rare earth doped tungsten trioxide is smaller than that of tungsten trioxide.

Fig. 4 shows diffuse reflectance UV-Vis absorption spectra of tungsten trioxide and rare earth doped tungsten trioxide nanowires. The properties of semiconductor are greatly dependant on band gap energy. The activity of the photocatalysts is strongly affected by band gap energy, because value of band gap energy can control rate of electron and hole recombination. The values of band gap energy of WO_3, Er-WO_3, Eu-WO_3, Pr-WO_3 and Nd-WO_3 samples , which calculated from UV-Vis spectra are tabulated in Table 1. The values are 2.9, 2.8, 2.7, 2.45 and 2.3 eV for WO_3, Er-WO_3, Eu-WO_3, Pr-WO_3 and Nd-WO_3 samples, respectively. Therefore, doping of rare earth has great effect of band gap energy of WO_3 nanowires.

Fig. 5. shows PL spectra of tungsten trioxide and rare earth doped tungsten trioxide nanowires. The results reveal that doping of rare earth has great effect on PL peak intensity of WO_3 nanowires. Therefore, doping of rare earth has great effect on e-h recombination rate and Nd-WO_3 sample has the lowest PL peak intensity and the lowest rate of *e-h* recombination rate, which are in agree with UV-Vis results and band gap values.

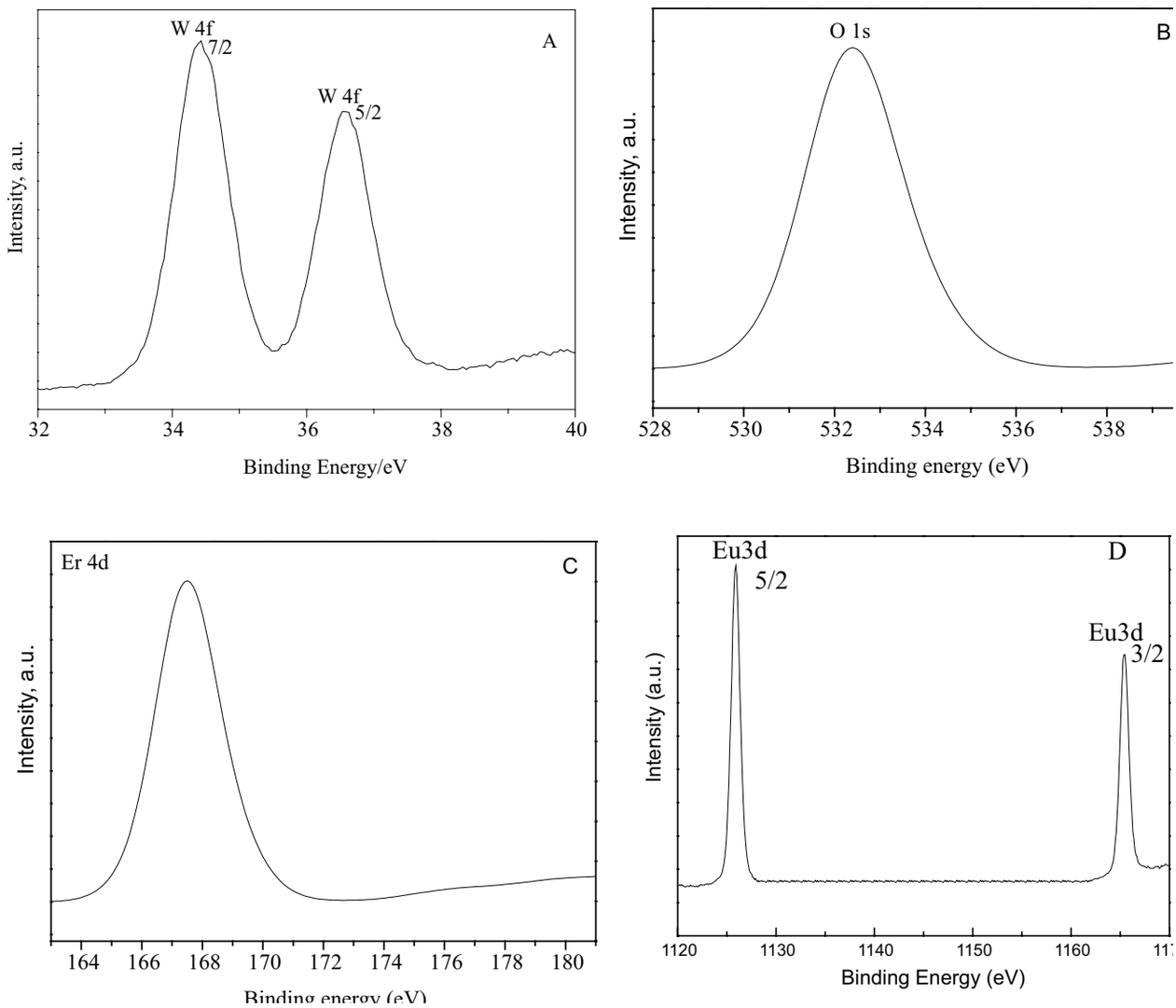

Fig. 2. XPS spectra of W(A), O(B), Er(C), Eu(D), Pr(E) and Nd(F) species of rare earth doped tungsten trioxide nanowires samples.

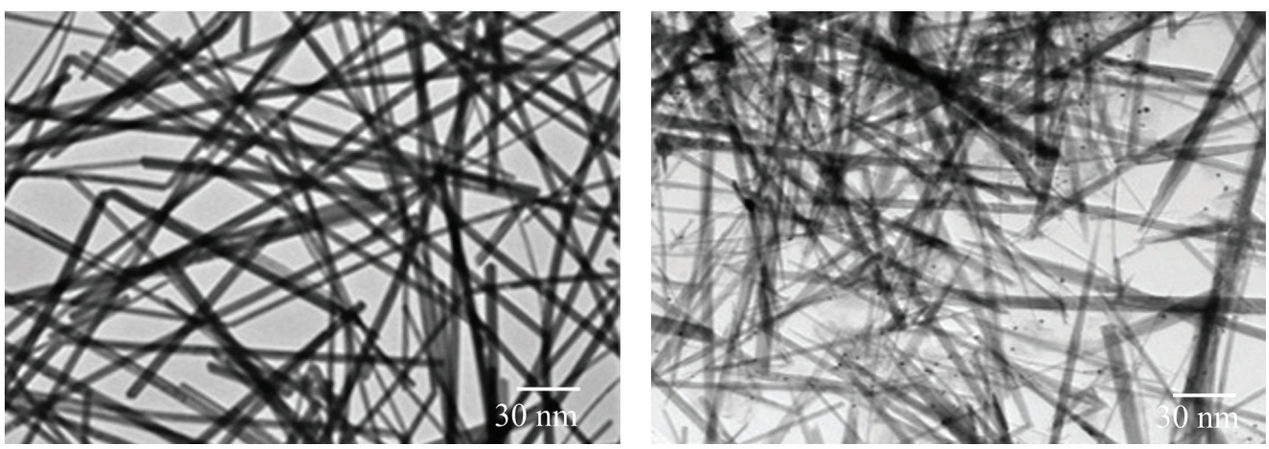

Fig. 3. TEM image of Tungsten trioxide (A) and 2 wt % Nd-WO_3 (B) nanowires.

Table 2
BET surface area and band gap of WO_3, Er-WO_3, Eu-WO_3, Pr-WO_3 and Nd-WO_3 samples

Sample	S_{BET} (m^2/g)	Band gap, eV
WO_3	90.00	2.90
2 wt % Er-WO_3	87.00	2.80
2 wt % Eu-WO_3	86.00	2.70
2 wt % Pr-WO_3	85.00	2.45
2 wt % Nd-WO_3	89.00	2.30

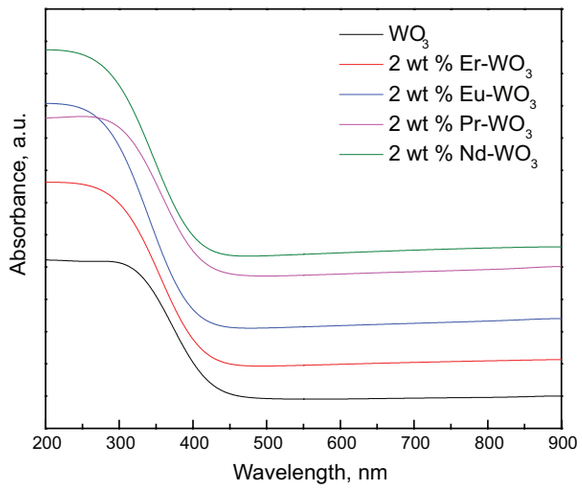

Fig. 4. Diffuse reflectance UV-Vis absorption spectra of tungsten trioxide and rare earth doped tungsten trioxide nanowires.

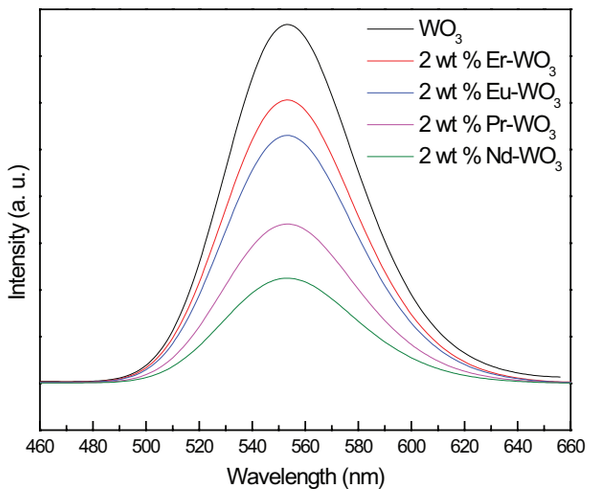

Fig. 5. PL spectra of tungsten trioxide and rare earth doped tungsten trioxide nanowires.

Fig. 6. shows transient photocurrent responses of tungsten trioxide and rare earth doped tungsten trioxide nanowires photocatalysts. The results reveal that the photocurrent density is increase in the following order WO_3 < Er-WO_3 < Eu-WO_3 < Pr-WO_3 < Nd-WO_3, which means the

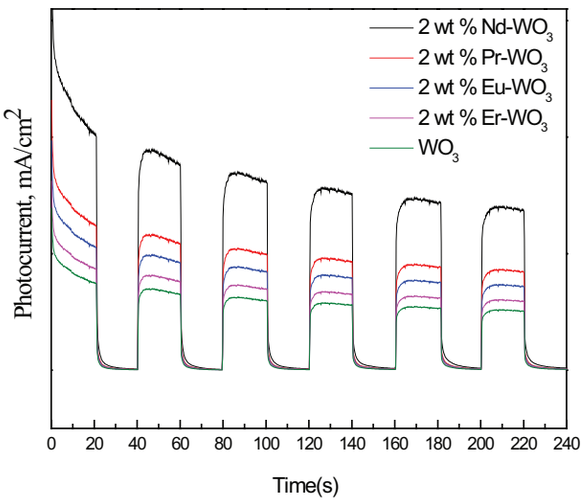

Fig. 6. Transient photocurrent responses of tungsten trioxide and rare earth doped tungsten trioxide nanowires photocatalysts.

e-h recombination rate is decreased in the following order WO_3 > Er-WO_3 > Eu-WO_3 >Pr-WO_3 > Nd-WO_3. The results of photocurrent density are very close to UV-Vis and PL spectra results.

3.2. Photocatalysts performances

Fig. 7 shows photocatalytic activity of tungsten trioxide and rare earth doped tungsten trioxide nanowires for thiophene removal efficiency %. The photocatalytic removal efficiency with the use of WO_3 is small (50%), this can be explained by the fact that WO_3 has wide band gap (2.90 eV) compared to values of the band gaps are earth doped tungsten trioxide nanowires samples. Photocatalytic removal efficiency of thiophene with the use of Er-WO_3, Eu-WO_3, Pr-WO_3 and Nd-WO_3 samples was at 65%, 75% , 85% and 100%, respectively. It is clear that the addition of rare earth elements increases photocatalytic removal efficiency of thiophene, due to decreased band gap, increased surface area and the increase of life time of e-h recombination rate as confirmed by PL and photocurrent density results.

To confirm the complete degradation of thiophene to CO_2, H_2O and SO_3, the obtained gases were passed through sodium hydroxide solution (0.2 M) and then to barium nitrate solution (0.2 M). The obtained precipitate 1 was determined by XRD as shown in Fig. 8. The XRD results confirm the presence of barium carbonate and so carbon dioxide is one of main products from degradation of thiophene. The precipitate 1 was added to nitric acid and the obtained precipitate was donate as precipitate 2 and was determined by XRD as shown in Fig. 9. The XRD results confirm the presence of barium sulfate and so SO_3 is one of main products from degradation of thiophene, which agree with published work [41,42,44,50,51].

The effect of the amount of added catalyst to the reaction was also studied. Fig. 10. Effect of photocatalyst dose of 2 wt % Pr- WO_3 nanowires on thiophene removal efficiency %. The photocatalytic removal efficiency of thiophene increased from 65 to 100% by increasing the dose from 0.4

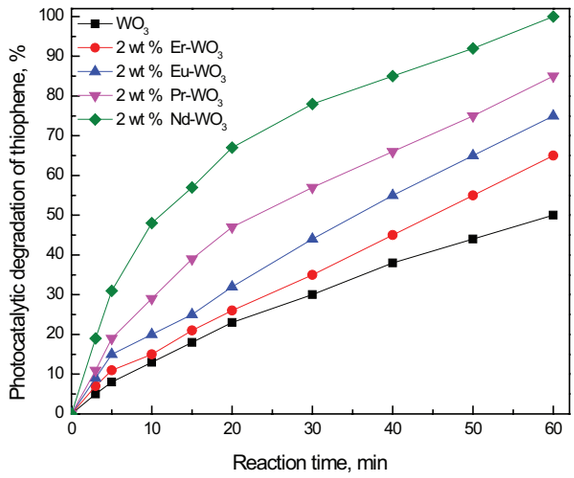

Fig. 7. Photocatalytic activity of tungsten trioxide and rare earth doped tungsten trioxide nanowires for thiophene removal efficiency %. Photocatalytic conditions are 60 min reaction time, visible light source of irradiation, 600 ppm initial sulfur concentration and 1.2 g/L dose of photocatalyst.

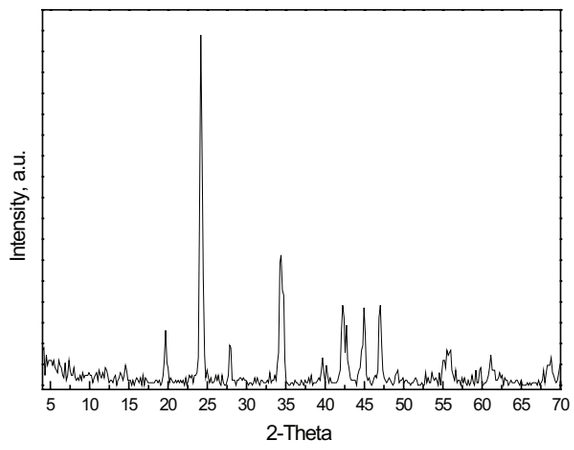

Fig. 8. XRD pattern of precipitate 1.

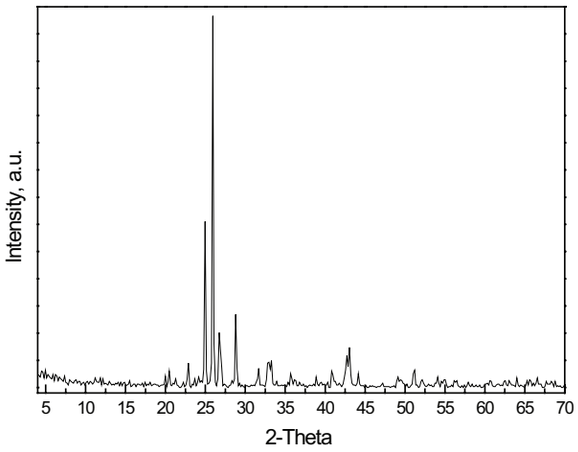

Fig. 9. XRD pattern of precipitate 2.

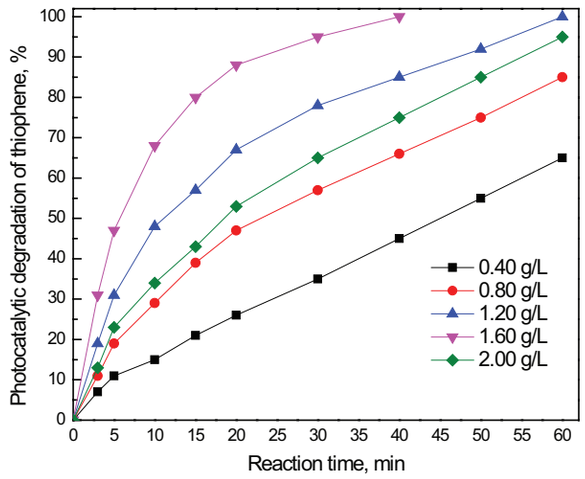

Fig. 10. Effect of photocatalyst dose of 2 wt % Nd-WO_3 nanowires on thiophene removal efficiency %. Photocatalytic conditions are 60 min reaction time, visible light source of irradiation, 600 ppm initial sulfur concentration and 2 wt % Nd-WO_3 used photocatalyst.

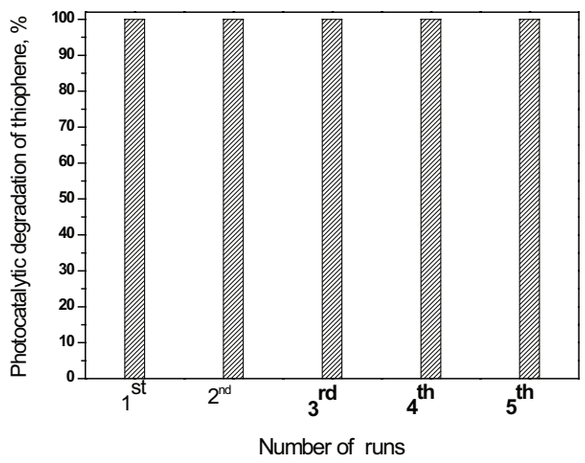

Fig. 11. Photocatalytic stability of 2 wt % Nd-WO_3 nanowires photocatalyst for photocatalytic degradation of thiophene. Photocatalytic conditions are 40 min reaction time, visible light source of irradiation, 600 ppm initial sulfur concentration, 2 wt % Nd-WO_3 used photocatalyst and 1.6 g/L dose of 2 wt % Nd-WO_3 Photocatalyst.

to 1.2 g/L, respectively. Reaction time required for a complete removal of thiophene decreased from 60 to 40 min by increasing the dose of 2 wt % Pr- WO_3 nanowires photocatalyst from 1.2 to 1.6 g/L, respectively. This may be due to increased number of available active sites by the increase in the dose of the photocatalyst. If the dose was raised above 1.2 g/L to a value of 1.6 g/L the photocatalytic 2 wt % Pr-WO_3 nanowires decreases from 100 to 95% and the reaction time increases from 40 to 60 min. the higher dose of photocatalyst beyond a certain point may result in hindering penetration of light to reach all active sites of the photocatalyst, which agree with published work [41,42,44,50,51].

A test on the possibility of the reuse of the catalyst was also performed. Fig. 11. shows photocatalytic stability of 2 wt % Pr-WO_3 nanowires photocatalyst for photocatalytic degradation of thiophene. The figure shows that the removal remains constant even if the catalyst was reused for additional four times showing great stability of the 2 wt % Pr-WO_3 nanowires photocatalyst, which agree with published work [41,42, 44, 50,51].

4. Conclusions

Tungsten trioxide nanowires were prepared successfully by a sol-gel technique. Rare earth doped tungsten trioxide nanowires were successfully prepared by a photoassisted deposition route. Crystallite size, texture structure and band gap energy of WO_3 nanowires can be controlled by control type of doped rare earth element. The photocatalytic activity of Rare earth doped tungsten trioxide nanowires is well correlated with BET surface area and band gap energy. Nd-WO_3 photocatalyst has the lowest band gap and particle size and has highest photocatalytic activity and specific surface area in regard to other rare earth doped WO_3 samples. This can be attributed to its individual properties of band gap, particle size and surface of texture.

Acknowledgments

This Project was funded by Center of Excellence in Environmental studies, under grant number (2/W/1435) and thanks MOHE and King Abdulaziz University (DSR) for technical and financial support.

References

[1] W. Teng-fei, Z. Ye, G. Hui, T. Ming-xing, Z. Li-gong, L.Ü. Zhanjun, L.I. Xue-kuan, Hydrodesulfurization of thiophene over Mo/AC catalyst presulfided by ammonium thiosulfate, J. Fuel Chem. Technol., 43 (2015) 202–207.

[2] Y. Boukoberine, B. Hamada, Thiophene hydrodesulfurization over CoMo/Al_2O_3-CuY catalysts: Temperature effect study, Arabian J. Chem., 9 (2016) S522–S527.

[3] T. Kabe, A. Ishiharam, H. Tajima, Hydrodesulfurization of sulfur containing polyaromatic compounds in light oil, Ind. Eng. Chem. Res., 31 (1992) 1577–1580.

[4] B.C. Gates, H. Topsoe, Reactivities in deep catalytic hydrode sulfurization: challenges, opportunities, and the importance of 4 methyldibenzothiophene and 4,6-dimethyl-dibenzothiophene, Polyhedron, 16 (1997) 3213–3217.

[5] X. Ma, K. Sakanishi, I. Mochida, Hydrodesulfurization reactivities of various sulfur compounds in diesel fuel, Ind. Eng. Chem., 33 (1994) 218–222.

[6] X. Ma, K. Sakanishi, T. Isoda, I. Mochida, Hydrodesulfurization reactivities of narrow-cut fractions in a gas oil, Ind. Eng. Chem. Res., 34 (1995) 748–754.

[7] E. Olguin-Orozco, M. Vrinat, L. Cedeno, J. Ramirez, M. Boroque, A.A. Lopez, The use of TiO_2–Al_2O_3 binary oxides as supports for Mo based catalysts in hydrodesulfurization of thiophene and dibenzothiophene, Appl. Catal. A., 165 (1997) 1–13.

[8] D.R. Kilanowski, H. Teeuwen, V.H.J. De Beer, B.C. Gates, B.C.A. Schuit, H. Kwart, Hydrodesulfurization of thiophene, benzothiophene, dibenzothiophene, and related compounds catalyzed by sulfided CoO–MoO_3/-Al_2O_3: low-pressure reactivity studies, J. Catal., 55 (1978) 129–137.

[9] L. Lin, Y. Zhang, Y. Kong, Recent advances in sulfur removal from gasoline by pervaporation, Fuel, 88 (2009) 1799–1809.

[10] I. Bettermann, C. Staudt, Desulphurization of kerosene: pervaporation of benzothiophene/n-dodecane mixtures, J. Membr. Sci., 343 (2009) 119–127.

[11] R. Qi, Y. Wang, J. Li, S. Zhu, Sulfur removal from gasoline by pervaporation: the effect of hydrocarbon species, Sep. Purif. Technol., 51 (2006) 258–264.

[12] M. Jain, D. Attarde, S. Gupta, Influence of hydrocarbon species on the removal of thiophene from FCC gasoline by using a spiral wound pervaporation module, J. Membr. Sci., 507 (2016) 43–54.

[13] M. Jain, D. Attarde, S. Gupta, Removal of thiophene from n-heptane/thiophene mixtures by spiral wound pervaporation module: Modelling, validation and influence of operating conditions, J. Membr. Sci., 490 (2015) 328–345.

[14] C. Song, An overview of new approaches to deep desulfurization for ultra-clean gasoline, diesel fuel and jet fuel, Catal. Today, 86 (2003) 211–263.

[15] X. Ma, L. Sun, C. Song, A new approach to deep desulfurization of gasoline, diesel fuel and jet fuel by selective adsorption for ultra-clean fuels and for fuel cell applications, Catal. Today, 77 (2002) 107–116.

[16] X. Ma, M. Sprague, L. Sun, C. Song, Deep desulfurization of liquid hydrocarbons by selective adsorption for fuel cell applications, Am. Chem. Soc., Div. Petrol. Chem. Prepr., 47 (2002) 48–49.

[17] X. Ma, L. Sun, Z. Yin, C. Song, New approaches to deep desulfurization of diesel fuel, jet fuel, and gasoline by adsorption for ultra-clean fuels and for fuel cell applications, Am. Chem. Soc., Div. Fuel Chem. Prepr., 46 (2001) 648–649.

[18] S. Velu, X. Ma, C. Song, Zeolite-based adsorbent for desulfurization of jet fuel by selective adsorption, Am. Chem. Soc., Div. Fuel: Chem.Prepr., 47 (2002) 447–448.

[19] S. Velu, X. Ma, C. Song, Fuel cell grade gasoline production by selective adsorption for removing sulfur, Am. Chem. Soc., Div. Petrol. Chem. Prepr., 48 (2003) 58–59.

[20] S. Velu, S. Watanable, X. Ma, C. Song, Development of selective adsorbent for removing sulfur from gasoline for fuel cell applications, Am. Chem. Soc., Div. Petrol. Chem. Prepr., 48 (2003) 56–57.

[21] H. Qi, S. Zhai, Z. Wang, B. Zhai, Q. An, Designing recyclable Cu/ZrSBA-15 for efficient thiophene removal, Micropor. Mesopor. Mater., 217 (2015) 21–29.

[22] K.L. Rock, Ultra-low sulfur gasoline via catalytic distillation, in: Proceedings of the Fifth International Conference on Refinery Processing. AIChE 2002 Spring National Meeting, New Orleans, LA, March, 11–14 (2002) 200–205.

[23] R. Rock, S. Shorey, Producing low sulfur gasoline reliably, AM-03 122, in: Proceedings of the NPRA 2003 Annual Meeting, San Antonio, TX, March 23–25, (2003).

[24] A. Bösmann, L. Datsevich, A. Jess, A. Lauter, C. Schmitz, P. Wasserscheid, Deep desulfurization of diesel fuel by extraction with ionic liquids, Chem. Commun., 23 (2001) 2494–2495.

[25] S.G. Zhang, Z.C. Zhang, Novel properties of ionic liquids in selective sulfur removal from fuels at room temperature, Green Chem., 4 (2002) 376–379.

[26] M. Mafi, B. Mokhtarani, M.R. Dehghani, Removal of thiophene from model diesel oil with nitrate based ionic liquids at several temperatures, J. Mol. Liq., 221 (2016) 1104–1110.

[27] S. Yu, F. Pan, S. Yang, H. Ding, Z. Jiang, B. Wang, Z. Li, X. Cao, Enhanced pervaporation performance of MIL-101(Cr) filled polysiloxane hybrid membranes in desulfurization of model gasoline: Chem. Eng. Sci., 135 (2015) 479–488.

[28] R. Konietzny, T. Koschine, K. Rätzke, C. Staudt, POSS-hybrid membranes for the removal of sulfur aromatics by pervaporation, Sep. Purif. Technol., 123 (2014) 175–182.

[29] R.A. Amaral, A.C. Habert, C.P. Borges, Activated carbon polyurethane membrane for a model fuel desulfurization by pervaporation: Mater. Lett., 137 (2014) 468–470.

[30] H. Qu, Y. Kong, H. Lv, Y. Zhang, J. Yang, D. Shi, Effect of crosslinking on sorption, diffusion and pervaporation of gasoline components in hydroxyl ethyl cellulose membranes: Chem. Eng. J., 157 (2010) 60–66.

[31] J. Chen, J. Li, R. Qi, H. Ye, C. Chen, Pervaporation performance of crosslinked polydimethyl siloxane membranes for deep desulfurization of FCC gasoline I. Effect of different sulfur species, J. Membr. Sci., 322 (2008) 113–121.
[32] C. Zhao, J. Li, R. Qi, J. Chen, Z. Luan, Pervaporation separation of n heptane/sulfur species mixtures with poly dimethyl siloxane membranes, Purif. Technol., 63 (2008) 220–225.
[33] M. Jain, D. Attarde, S. Gupta, Removal of thiophenes from FCC gasoline by using a hollow fiber pervaporation module: Modeling, validation, and influence of module dimensions and flow directions, Chem. Eng. J., 308 (2017) 632–648.
[34] Z. Yang, W. Zhang, T. Wang, J. Li, Improved thiophene solution selectivity by Cu^{2+}, Pb^{2+} and Mn^{2+} ions in pervaporative poly [bis (p-methylphenyl) phosphazene] desulfurization membrane, J. Membr. Sci., 454 (2014) 463–469.
[35] K. Liu, C.-J. Fang, Z.-Q. Li, M. Young, Separation of thiophene/n-heptane mixtures using PEBAX/PVDF-composited membranes via pervaporation, J. Membr. Sci., 451 (2014) 24–31.
[36] L. Lin, M. Dong, C. Liu, H. Sun, L. Zhang, C. Zhang, P. Deng, Y. Li, Building movable bridges in membrane matrix by polyrotaxane crosslinking for sulfur removal, Mater. Lett., 126 (2014) 59–62.
[37] Z. Yang, T. Wang, X. Zhan, J. Li, J. Chen, Poly [bis(p-methylphenyl) phosphazene] pervaporative membranes for separating organo sulfur compounds from n-heptane and its surface functionalization, Ind. Eng. Chem. Res., 52 (2013) 13801–13809.
[38] L. Lin, A. Wang, M. Dong, Y. Zhang, B. He, H. Li, Sulfur removal from fuel using zeolites/polyimide mixed matrix membrane adsorbents, J. Hazard. Mater., 203 (2012) 204–212.
[39] G. Liu, T. Zhou, W. Liu, S. Hu, F. Pan, H. Wu, Z. Jiang, B. Wang, J. Yang, X. Cao, Enhanced desulfurization performance of PDMS membranes by incorporating silver decorated dopamine nanoparticles, J. Mater. Chem. A., 2 (2014) 12907–12917.
[40] B. Mokhtarani, H. Mansourzareh, H.R. Mortaheb, Phase behavior of nitrate based ionic liquids with thiophene and alkanes, Ind. Eng. Chem. Res., 53(3) (2014) 1256–1261.
[41] R.M. Mohamed, E.S. Aazam, Preparation and characterization of core–shell polyaniline/mesoporous Cu_2O nanocomposites for the photo catalytic oxidation of thiophene, Appl. Catal. A., 480 (2014) 100–107.
[42] E.S. Aazam, Visible light photo catalytic degradation of thiophene using Ag–TiO_2/multi-walled carbon nano tubes nano composite, Ceram. Int., 40 (2014) 6705–6711.
[43] F. Lina, Z. Jiangb, N. Tangb, C. Zhangb, Z. Chenb, T. Liub, B. Donga, Photocatalytic oxidation of thiophene on RuO_2/SO_{42}-TiO_2: Insights for cocatalyst and solid-acid, Appl. Catal. B., 188 (2016) 253–258.
[44] E. Baeissa, Environmental remediation of thiophene solution by photocatalytic oxidation using NiO/$AgInS_2$ nanoparticles, J. Ind Eng. Chem., 20 (2014) 3270–3275.
[45] M.Y. Abdelaala, R.M. Mohamed, Environmental remediation from thiophene solution by photocatalytic oxidation using a Pd/ZrO_2–chitosan nanocomposite, Ceram. Int., 40 (2014) 7693–7699.
[46] X. Gao, F. Fu, L. Zhang, W. Li, The preparation of Ag–$BiVO_4$ metal composite oxides and its application in efficient photocatalytic oxidative thiophene, Phys. B., 419 (2013) 80–85.
[47] F.C. Marques, M.C. Canela, A.M. Stumbo, Use of TiO_2/Cr-MCM-41 molecular sieve irradiated with visible light for the degradation of thiophene in the gas phase, Catal. Today., 133–135 (2008) 594–599.
[48] G. Dedual, M.J. MacDonald, A. Alshareef, Z. Wub, D.C.W. Tsang, A.C.K. Yip, Requirements for effective photocatalytic oxidative desulfurization of a thiophene-containing solution using TiO_2, J. Environ. Chem. Eng., 2 (2014) 1947–1955.
[49] L. Wang, H. Cai, S. Li, N. Mominou, Ultra-deep removal of thiophene compounds in diesel oil over catalyst TiO_2/Ni-ZSM-5 assisted by ultraviolet irradiating, Fuel, 105 (2013) 752–756.
[50] R.M. Mohamed, E.S. Aazam. New visible-light Pt/PbS nanoparticle photocatalysts for the photocatalytic oxidation of thiophene, Clean Soil Air Water, 42 (2014) 1–6.
[51] L. Xue, D. Zhang, Y. Xu, X. Liu, Adsorption of thiophene compounds on MoO_3/x-Al_2O_3 catalysts with different mesopore sizes, Micropor. Mesopor. Mater. In press. (2016) doi. org/10.1016/j.micromeso.2016.03.004.
[52] M. Barmala, A.Z. Moghadam, M.R. Omidkhah, Increased photo-catalytic removal of sulfur using titania/MWCNT composite, J. Cent. South Univ., 22 (2015) 1066–1070.
[53] Z.G. Zhao, M. Miyauchi, Nanoporous-walled tungsten oxide nanotubes as highly active visible-light-driven photocatalysts, Angew. Chem. Int. Ed., 47 (2008) 7051–7055.
[54] V. Likodimos, D.D. Dionysiou, P. Falaras, CLEAN WATER: water detoxification using innovative photocatalysts, Rev. Environ. Sci. Bio-Technol., 9 (2010) 87–94.
[55] T. Fotiou, T.M. Triantis, T. Kaloudis, A. Hiskia, Evaluation of the photocatalytic activity of TiO_2 based catalysts for the degradation and mineralization of cyanobacterial toxins and water off-odor compounds under UV-A, solar and visible light, Chem. Eng. J., 261 (2015) 17–26.
[56] R. Abe, H. Takami, N. Murakami, B. Ohtani, Pristine simple oxides as visible light driven photocatalysts: highly efficient decomposition of organic compounds over platinum-loaded tungsten oxide, J. Am. Chem. Soc., 130 (2008) 7780–7781.
[57] T. Arai, M. Horiguchi, M. Yanagida, T. Gunji, H. Sugihara, K. Sayama, Complete oxidation of acetaldehyde and toluene over a Pd/WO_3 photocatalyst under fluorescent- or visible-light irradiation, Chem. Commun., (2008) 5565–5567.
[58] T. Arai, M. Yanagida, Y. Konishi, Y. Iwasaki, H. Sugihara, K. Sayama, Promotion effect of CuO co-catalyst on WO_3-catalyzed photo degradation of organic substances, Catal. Commun., 9 (2008) 1254–1258.
[59] Q. Xiang, G.F. Meng, H.B. Zhao, Y. Zhang, H. Li, W.J. Ma, J.Q. Xu, Au nanoparticle modified WO_3 nanorods with their enhanced properties for photocatalysis and gas sensing, J. Phys. Chem. C, 114 (2010) 2049–2055.
[60] Y.H. Kim, H. Irie, K. Hashimoto, A visible light-sensitive tungsten carbide/tungsten trioxde composite photocatalyst, Appl. Phys. Lett., 92 (2008) 182107-1–182107–3.
[61] J. Brillet, J.-H. Yum, M. Cornuz, T. Hisatomi, R. Solarska, J. Augustynski, Highly efficient water splitting by a dual absorber tandem cell, Nat. Photonics., 6 (2012) 824–828.
[62] B. Cole, B. Marsen, E. Miller, Y. Yan, K. Jones, Evaluation of nitrogen doping of tungsten oxide for photoelectrochemical water splitting, J. Phys. Chem. C, 112 (2008) 5213–5220.